Locating RFI Source by Integrating Ascending and Descending Passes Based on SAR Raw Data

Zewen Fu ⓘ, Ning Li ⓘ, *Member, IEEE*, and Zhengwei Guo ⓘ

Abstract—The existence of radio frequency interference (RFI) significantly affects the quality of synthetic aperture radar (SAR) images. Locating RFI source serves as a component of electromagnetic situational awareness, which provides preliminary information for intelligent anti-interference. In this article, an RFI source localization method was proposed. Specifically, the SAR raw data both in ascending and descending passes were integrated to obtain the localization information of RFI. The localization index (LI) was first proposed to locate the RFI source after RFI detection and extraction. Subsequently, the location of the RFI source is determined by referring to the LI and the orbit inclination of the satellite-borne SAR based on radiation pattern weighing (RPW) in azimuth. Finally, the localization accuracy of the proposed method in both side-looking and squint situations is verified through simulation experiments. Based on the SAR level-0 raw data of sentinel-1 in Dubai and Jinan, the localization results show that the RFI source are near the city center or the airport. It provides a high-precision and convenient RFI source localization solution for anti-interference as well as monitoring RFI, and theoretical analyses indicate significant improvements in localization accuracy compared to the traditional X-mark method.

Index Terms—Localization index (LI), orbit inclination, radiation pattern weighing (RPW), radio frequency interference (RFI), synthetic aperture radar (SAR).

I. INTRODUCTION

A. Background

RADIO frequency interference (RFI) can seriously affect the interpretation of synthetic aperture radar (SAR) images [1], [2], [3], [4], [5]. With the continuous development of science and technology, various electronic devices are constantly emerging, resulting in a complex electromagnetic environment. Moreover, this electromagnetic environment has been steadily deteriorating over time [6]. The occurrence of RFI is mainly caused by spectrum allocation issues, and electromagnetic spectrum resources are becoming increasingly scarce. Consequently, signals emanating from sources unavoidably intertwine with

The authors are with the School of Computer and Information Engineering, Henan University, Kaifeng 475004, China, also with the Henan Key Laboratory of Big Data Analysis and Processing, Kaifeng 475004, China, and also with the Henan Province Engineering Research Center of Spatial Information Processing, Kaifeng 475004, China (e-mail: fuzewen@henu.edu.cn; hedalining@henu.edu.cn; gzw@henu.edu.cn).

those received by SAR, resulting in a notable degradation in image quality [7], [8], [9], [10]. The SAR images contaminated by RFI are shown in Fig. 1.

RFI sources may originate from various electronic devices in maritime or terrestrial domain, significantly impacting the observational performance of SAR, so the surveillance and awareness for maritime and terrestrial domain RFI are of great significance. On the one hand, most RFI are generated from terrestrial signal towers, coastal radars, airports, and more. For maritime targets, such as ships, noncooperative surveillance systems, and more, rarely broadcast, e.g., identification or location information. Therefore, for the abovementioned RFI sources, continuous monitoring during peacetime or wartime to obtain information such as their geographical location can provides valuable information to decision makers.

To mitigate the impact of electromagnetic interference on SAR images, numerous algorithms for RFI suppression have been proposed by researchers, which can suppress RFI in different situations. Nonetheless, most existing algorithms suppress RFI after the SAR system receives the RFI. By this point, the RFI has already affected the useful signal. Utilizing the aforementioned algorithm for RFI suppression results in the inevitable loss of useful signals. Therefore, preventing RFI signals from entering the receiver can fundamentally solve the impact of RFI, which is more practical than RFI suppression.

SAR active anti-interference strategy is based on RFI perception and involves program-controlled agility processing of the carrier frequency, repetition frequency, and other related parameters of the SAR system [11]. The sentinel-1 earth observation satellite has an interference suppression module, which can suppress RFI entering the SAR receiver to a certain extent and provides a probability distribution diagram of possible RFI to the system [12]. However, active anti-interference of SAR requires precise parameters of RFI source, such as the location of RFI source. Obtaining higher RFI source localization accuracy can effectively improve anti-interference performance, and locating RFI source plays a vital role in the field of anti-interference. In summary, obtaining the localization information of RFI sources is crucial.

B. Previous Work

Localization of RFI can be generally divided into active location and passive location. While in the field of electronic reconnaissance, passive location is the mainstream direction.
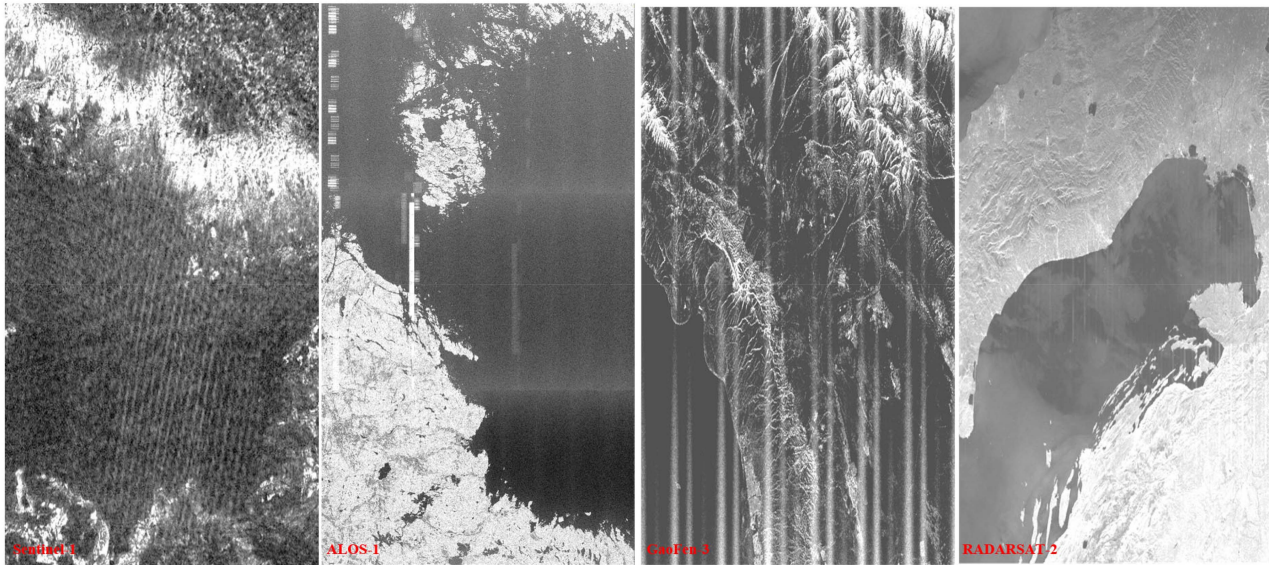
Fig. 1.　Example case of the SAR images contaminated by RFI.

Passive location methods are generally divided into three categories. The parameter estimation, signal sensing and the concept of synthetic aperture are utilized to locate the RFI source.

Until now, researchers have proposed a variety of the localization algorithms for RFI source, which can use parameters such as phase difference [13], time difference of arrival (TDOA) [14], frequency difference of arrival (FDOA) [15], Doppler rate [16], and direction of arrival (DOA) [17] to complete the interference source location. For example, Park et al. [18] introduced a new RFI localization method by using beamforming and DOA. Dempster and Cetin [19] focused on Global Navigation Satellite Systems, utilized sensor nodes to receive signal strength, DOA, TDOA, or combine DOA and FDOA to estimate the location of RFI sources. Li et al. [20] proposed a novel RFI localization approach using covariance matrix augmentation in synthetic aperture interferometric radiometry. Steeb et al. [21] proposed a localization algorithm for interferometric arrays with low array beam sidelobes, adaptable for use in both the near field and far field. Jin et al. [22] proposed a multiple snapshot difference method to further reduce the RFI source geolocation bias based on DOA. Zhu et al. [23], [24] proposed a series of localization algorithms based on joint sparse recovery. The above method relies on the quality and completeness of signal reception. When the parameter estimation accuracy is limited, the localization accuracy of RFI source will be affected

In recent years, some algorithms have incorporated the use of synthetic aperture imaging into RFI source localization. Zhang [25], [26] et al. proposed an emitter localization algorithm based on passive synthetic aperture in the spaceborne model. Wang et al. [27] presented a radiation-source localization algorithm based on a long synthetic aperture. The above methods have achieved high passive localization accuracy, but they are constrained by the signal transmit-receive unit and may not be directly applicable to RFI source location in the SAR field, measured SAR data has not yet been applied.

For the localization of RFI source based on SAR data, Sørensen detected and localized RFI signals automatically in sentinel-1 level-1 images, this method improved maritime domain awareness greatly [28]. Yang studied the localization model and method of ground-based pulse emitters using SAR as the observation platform, and it achieved near-optimal localization accuracy [29]. The Italian remote sensing company ARESYE produced an interference map to roughly geotag C-band ground-based interference emitters observed by sentinel-1 [30].

The idea of integrating ascending and descending passes has been applied in various fields such as agriculture, deformation monitoring, and earth observation. Banks et al. [31] reduced ascending and descending passes bias in SMOS salinity data demonstrated by observing westward-propagating features in the South Indian Ocean. Kumar et al. [32] estimated the glacier surface velocity in the Himalayas by integrating ascending and descending passes based on SAR data. The application of the ascending and descending passes mentioned above has inspired researchers to integrate ascending and descending passes for locating interference sources based on SAR data. Dan proposed using ascent and descent observations to create the X-mark for rough localization of the RFI sources, but this method has not received analysis and promotion [33]. Based on the X-mark method of Dan, Leng et al. analyzed the accuracy of the X-mark method, the ascending and descending passes are utilized to locate the RFI sources in sentinel-1 images, offering an intriguing and innovative approach. Leng et al. [34] pointed out that the spatial accuracy is within a diamond-shaped area of approximately 89 square km. Due to the complex geometric model of SAR, the aliasing of useful signals and RFI signals, the localization accuracy of these methods is limited, and further exploration is warranted. In summary, RFI source localization technology based on SAR data is still evolving. With the increasingly complex electromagnetic environment, the demand for RFI source

location based on SAR data is on the rise. Additionally, the ever-changing international environment underscores the importance of RFI source location in the advancement of national defense capabilities. Thus, the exploration of RFI source location based on SAR data holds significant relevance.

C. Solution and Contributions of This Article

In this article, an RFI source localization method by integrating SAR raw data both in ascending and descending passes was proposed. In this scheme, the localization index (LI) was first proposed to locate the RFI source after RFI detection and extraction. Subsequently, the location of the RFI source is determined by referring to the LI and the orbit inclination of the satellite-borne SAR based on radiation pattern weighing (RPW) in azimuth. The localization accuracy of the proposed scheme in different situations is verified through simulation experiments, and the localization accuracy significantly improved compared to traditional algorithms based on experimental results of sentinel-1 raw data.

The main contributions of this article are summarized as follows.

1) The concept of LI is first proposed, and the location of the RFI source is determined by referring to the LI and the orbit inclination of the satellite-borne SAR after RFI detection and extraction. The proposed localization scheme based on LI effectively achieves higher accuracy in location than traditional X-mark method.

2) The idea of RPW is applied to the fitting of antenna gain for the first time, and the spatial positional relationships between RFI sources and the beam irradiation area of SAR system are briefly analyzed. Higher accuracy of LI can be calculated based on RPW.

3) The simulation experiments on the location of RFI source in both side-looking and squint situations are conducted, we find that it is feasible to obtain meter-level localization accuracy under proper SAR observation geometry and ideal conditions.

4) SAR level-0 raw data of sentinel-1 are utilized to explore and analyze the location of RFI sources. The proposed scheme is implemented in Dubai and Jinan regions, resulting in the identification of potential geographical locations of RFI sources in raw data contaminated by RFI. It demonstrates that the proposed scheme can be effectively applied to spaceborne SAR data.

D. Organization of This Article

This rest of this article is organized as follows. In Section II, the signal model and characteristic of RFI are introduced. Section III shows the RFI source localization workflow. Then, the experiments are shown in Section IV. Finally, Section V concludes this article

II. SIGNAL TRANSMISSION MODEL AND CHARACTERISTIC

In SAR system, the receiver not only receives the signal transmitted by SAR system, but also receives the RFI signal.
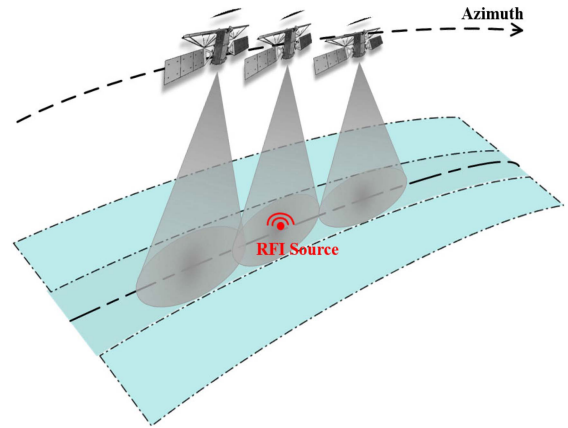

Fig. 2.   RFI dispersion along with the synthetic aperture.

Therefore, the SAR raw data is aliased with RFI signals, and RFI seriously affects the ability to observe the earth of SAR. The SAR geometric model is shown in Fig. 2.

The signals exist in two-dimensional time domain. After quadrature demodulation and digital sampling, the raw data received by SAR system can be written as

$$S\ (\tau, \eta) =\ X\ (\tau, \eta) + I\ (\tau, \eta) + N\ (\tau, \eta) \tag{1}$$

where $X(\tau, \eta)$ represents the useful signal, $I(\tau, \eta)$ represents the RFI signal, and $N(\tau, \eta)$ represents the system noise, τ and η denote the range fast time and the azimuth slow time, respectively.

In general, the RFI signal is different from backscatter coefficient of the general earth's surface, and it has stronger power than the normal backscatter coefficient. The RFI signal model can be expressed as

$$I\ (\tau, \eta) = \sum_{n=1}^{N} A_n\ (\eta)\ \cdot \exp\left(2j\pi f_n \tau + \varphi_n\right) \tag{2}$$

where N represents the number of RFI signals, A_n, f_n, K_n and φ_n represent the amplitude, frequency, chirp rate and phase of the nth RFI signals, respectively. T_I denotes the RFI receiving duration, and τ_I is the center time of RFI receicing duration.

The characteristics of RFI are generally more obvious in the echo domain. When there RFI in the signal received by the SAR system, the power of the RFI signal is generally stronger than that of the normal useful signal. After the accumulation of the synthetic aperture time, the RFI signal has a significant feature. Therefore, according to the different characteristics of the RFI signal and the useful signal, it can be judged whether there is RFI in the echo received by the SAR system, and the RFI can be extracted to facilitate subsequent further processing of the RFI.

In addition, the location of the RFI source and the SAR system are also different. According to the location of the RFI source, the possible RFI threats to the SAR system can be divided into ground-based RFI sources and space-based RFI sources. Since this article considers that the presence of RFI is persistent, only ground-based RFI sources are considered. There are two types of spatial positional relationships between RFI sources and the beam irradiation area of SAR system as follows.
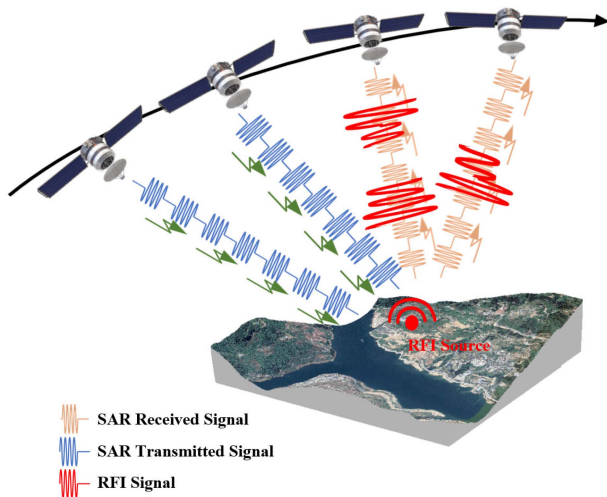
Fig. 3. The schematic diagram of echo signal and RFI signal.

1) RFI sources are located in the SAR beam irradiation area, the beam of RFI sources points to the antenna of main lobe or side lobe in the SAR system.
2) RFI sources are located outside the irradiation area of the SAR beam, and the beam of RFI sources points to the antenna of main lobe or side lobe in the SAR system.

It should be pointed out that due to the change of operating distance and the energy loss of signal transmission, there are certain differences in the influence of RFI sources at different locations on SAR. However, as the SAR system approaches the RFI source, the intensity of the RFI signal is constantly increasing. The strength of the RFI signal is constantly changing, and the signal strength at the center of the RFI source is the highest. The RFI signals enter the receiver irregularly, but the energy distribution conforms to the above rules. The schematic diagram of SAR signal and RFI signal transmission is shown in Fig. 3.

Based on the phenomena described above and different signal characteristics, the RFI source localization algorithm can be further explored and optimized.

III. RELATED WORKS

There is a significant difference between SAR echo signal and the RFI signal, which has been analyzed in our previous research. RFI in the range-frequency domain has a relatively stable frequency in the slow time direction, and its amplitude appears as some parallel straight lines, as shown in Fig. 4(a). It is clear that RFI has low-rank properties in the slow time direction. For further verification, the eigenvalue decomposition of Fig. 4(a) is performed, and the corresponding results are shown in Fig. 4(b). The eigenvalues reflect the energy of different components in the SAR echo and the structural redundancy of the matrix. As can be observed, only a few large eigenvalues are related to RFI, which further illustrates the low-rank feature of RFI in the range-frequency domain. Based on the above features, a theoretical foundation can be established for the RFI detection and extraction.
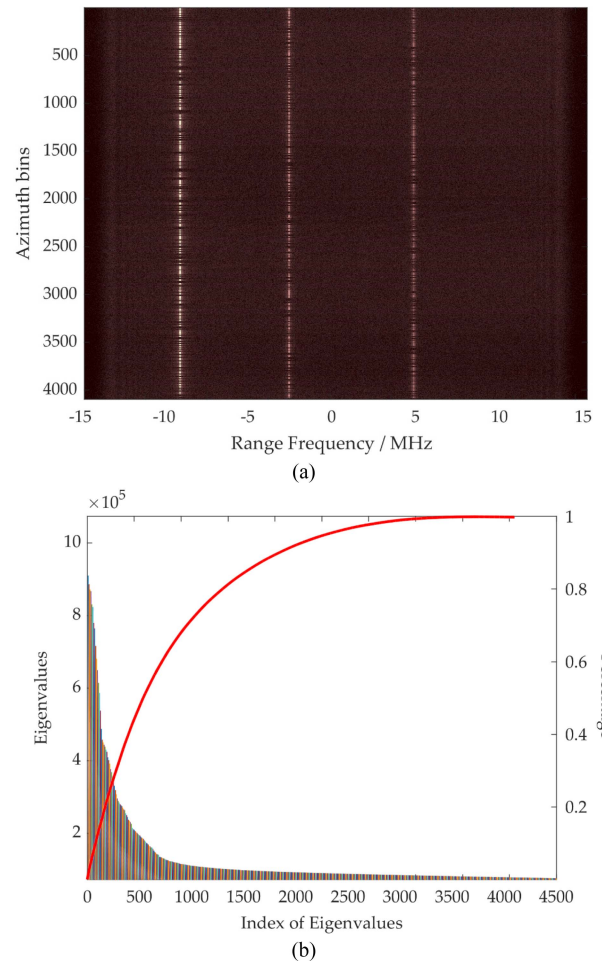

Fig. 4. Structural Analysis of RFI in Range-Frequency Domain. (a) Spectrogram of SAR echoes contaminated by RFI. (b) Eigenvalue sequences and analysis corresponding to (a).

Dan first proposed the traditional X-mark method, and based on this work, Leng proposed an RFI detection and localization method for C-band sentinel-1 SAR images. This method utilized the different characteristics of RFI in dual-polarization SAR data, and the RFI index (RFII) was proposed to complete the RFI detection. Finally, the approximate location of the RFI source was obtained through the ascending and descending passes SAR images. The above description is the X-mark method.

For the sentinel-1 SAR data, a rough localization method is as follows.

The orientation of RFI is determined by the azimuth direction or the flight direction. One single image cannot give a precise position since it is ambiguous in the azimuth direction. However, if the same RFI ground source is recorded by two images of different passes, the ambiguity can be eliminated by the intersection of two images with different azimuth directions. The orbital inclination θ of sentinel-1 is 98.18°, the level inclination of the RFI between the range is approximately 8.18°. The area of this diamond is as follows:

$$T \approx L^2 \left(\tan\left(\theta - 90°\right) + \frac{1}{\tan 2\theta} \right) \tag{3}$$
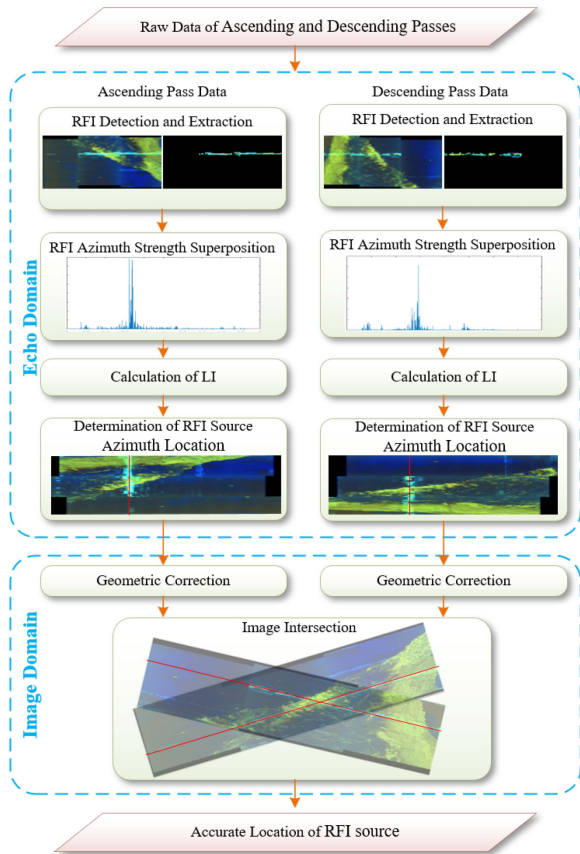
Fig. 5.   Main flowchart of the proposed method.

where L is the synthetic aperture length. Thus, the localization result is simply calculated.

In summary, the above is the process of RFI detection and location. It can be seen that the accuracy of location needs further improvement, and it can only be located in a large area of approximately 89 square km, unable to obtain the precise location of the RFI source. Therefore, based on the idea of this algorithm, we have continued to conduct more in-depth research.

IV. PROPOSED METHOD

To obtain the location information of the RFI source and facilitate subsequent measures to avoid RFI entering the SAR receiver, a RFI source localization method is proposed. The proposed method first detects and extracts the RFI. Then the LI is proposed to obtain the highest probability azimuth location of the RFI source. Finally, locates the RFI source according to the orbit inclination and other information of the ascending and descending passes data. The main flowchart of the proposed method is shown in Fig. 5.

A. RFI Detection and Extraction

According to the characteristics of the RFI signal, it can be known that the RFI generally has relatively strong power, and the eigenvalues corresponding to the RFI signal are greater than the eigenvalues of the SAR signal.

Consider N_r and N_a as sampling points in the range and azimuth respectively, and substitute $s_i(\tau_r)$, $r = 1, 2 \ldots, N_r$, $i = 1, 2, \ldots, N_a$ into the following matrix structure:

$$\mathbf{S} = \begin{bmatrix} s_i(\tau_1) & s_i(\tau_2) & s_i(\tau_3) & \cdots & s_i(\tau_M) \\ s_i(\tau_2) & s_i(\tau_3) & s_i(\tau_4) & \cdots & s_i(\tau_{M+1}) \\ s_i(\tau_3) & s_i(\tau_4) & s_i(\tau_5) & \cdots & s_i(\tau_{M+2}) \\ \vdots & \vdots & \vdots & \ddots & \cdots \\ s_i(\tau_L) & s_i(\tau_{L+1}) & s_i(\tau_{L+2}) & \cdots & s_i(\tau_{M+L-1}) \end{bmatrix} \tag{4}$$

where L is the dimension of the subspace matrix, and $M = N_r + L - 1$. The covariance matrix $\hat{\boldsymbol{R}} \in \mathbb{C}^{L \times L}$ can be expressed as

$$\hat{\mathbf{R}} = \mathbf{S}\mathbf{S}^H \tag{5}$$

Then the eigenvalue decomposition can be obtained: $\hat{\mathbf{R}} = \mathbf{S}\mathbf{S}^H = \mathbf{E}\boldsymbol{\Lambda}\mathbf{E}^H$. Where $\boldsymbol{\Lambda} = \mathbf{diag}(\boldsymbol{\gamma}_1, \boldsymbol{\gamma}_2, \boldsymbol{\gamma}_3, \cdots, \boldsymbol{\gamma}_L), \gamma$ is the eigenvalue, and the eigenvector can be expressed as $\mathbf{E} = [\epsilon_1, \epsilon_2, \epsilon_3, \ldots, \epsilon_L]$.

Repeat the above process in a pulse-by-pulse manner, and after each processing of the eigenvalue decomposition to obtain the maximum eigenvalue, the maximum eigenvalue sequence can be obtained, which can be expressed as

$$\boldsymbol{\Phi}(i) = [\xi_1, \xi_2 \cdots \xi_{N_a}] \tag{6}$$

where $\xi_i = \max\{\gamma_1, \gamma_2, \gamma_3, \cdots, \gamma_L\}$, and one ξ_i can be obtained after each eigenvalue decomposition. When the value is greater than the threshold δ, it is considered that there is RFI in the signal, and when the value is less than the threshold δ, there is no RFI. The threshold δ is generally taken as 2.

In this step, it is detected whether there is RFI in the signal received by the SAR system through a matrix operation, which facilitates further extraction and location of the RFI in the future.

Since the useful signal will affect the localization accuracy of the RFI source in subsequent operations, this step sets the non-RFI signal part to zero, so that only the RFI signal exists in the target matrix, which can be expressed as

$$\bar{\boldsymbol{\Phi}}(i) = 0, \bar{\boldsymbol{\Phi}}(i) < \delta. \tag{7}$$

Low rank sparse decomposition is performed to remove SAR echo and retain the RFI signal. It can be considered that there are only RFI signals. In the subsequent analysis and location of RFI, the influence of useful signals is eliminated, and the localization accuracy is further improved.

B. RFI Source Location

Azimuth superposition is performed on the signal after RFI extraction to obtain the strength value $\mathbf{P}$ of the RFI signal in the azimuth.

$$\mathbf{P} = \left[\sum_{r=1}^{N_r} s_1(\tau_r), \sum_{r=1}^{N_r} s_2(\tau_r), \cdots, \sum_{r=1}^{N_r} s_{N_a}(\tau_r) \right]. \tag{8}$$

Currently, $\mathbf{P}$ represents the strength of the RFI signal at each azimuth slow time in the matrix, and the variation trend of the RFI signal is fitted according to the strength, and the

influence of phase is ignored, the superposition of signal strength in amplitude is considered.

Then, the RPW is performed. Due to the fact that the data extracted from RFI is inevitably scattered compared to the RFI data received passively under ideal conditions, it is difficult to achieve the intensity change trend under ideal conditions. At this point, it is necessary to use fitting methods to find the location of the RFI source. Let a given central conic section have equation:

$$\mathbf{Q}\left(x,y\right) = Ax^2 + Bxy + Cy^2 + Dx + Ey + F = 0. \quad (9)$$

Given the values of N_a data points and fitting them to minimize errors in a certain sense, mathematical analysis is performed on the above equation, and set the objective function to I, and the best-fitting a scatter is estimated by minimizing I

$$I = \sum_{i=1}^{N_a} \mathbf{Q}^2\left(i, p_i\right) \quad (10)$$

where p_i represents the strength of the i-th pulse. By solving the six coefficients of (9), $I = $ min can be satisfied. Obtain the optimal solution based on various constraints, i.e., obtain the optimal fitting result. We solve the following equation system:

$$\begin{cases} \frac{\partial I}{\partial A} = 0 \\ \frac{\partial I}{\partial B} = 0 \\ \frac{\partial I}{\partial C} = 0 \\ \frac{\partial I}{\partial D} = 0 \\ \frac{\partial I}{\partial E} = 0 \\ \frac{\partial I}{\partial F} = 0 \end{cases}. \quad (11)$$

To solve the above equation system, to avoid zero solutions, we set $A = 1$, and incorporate it into I. We can obtain

$$\begin{cases} \frac{\partial I}{\partial B} = 0 \\ \frac{\partial I}{\partial C} = 0 \\ \frac{\partial I}{\partial D} = 0. \\ \frac{\partial I}{\partial E} = 0 \\ \frac{\partial I}{\partial F} = 0 \end{cases} \quad (12)$$

A set of solutions is obtained

$$\mathbf{coef}^1 = [A_1, B_1, C_1, D_1, E_1, F_1]. \quad (13)$$

Similarly, $B = 1, C = 1, D = 1, E = 1, F = 1$ are set to obtain five sets of solutions

$$\mathbf{coef}^2 = [A_2, B_2, C_2, D_2, E_2, F_2]$$
$$\mathbf{coef}^3 = [A_3, B_3, C_3, D_3, E_3, F_3]$$
$$\mathbf{coef}^4 = [A_4, B_4, C_4, D_4, E_4, F_4]$$
$$\mathbf{coef}^5 = [A_5, B_5, C_5, D_5, E_5, F_5]. \quad (14)$$
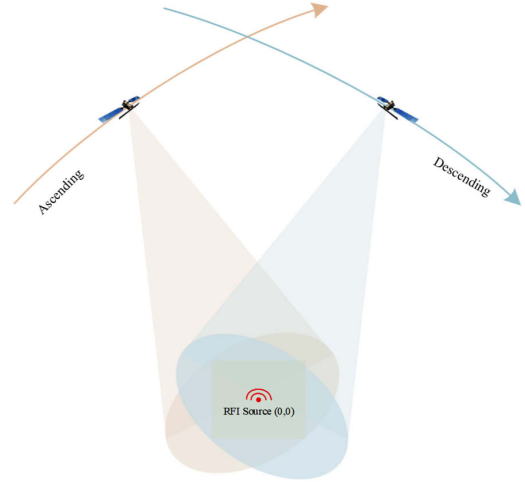

Fig. 6. Geometric model of the simulation experiments.

In order to make the fitting results more stable, the objective function I_n is determined

$$I_n = \sum_{j=1}^{N_a} \left(A_n j^2 + B_n j p_j + C_n p_j{}^2 + D_n j + E_n p_j + F_n\right). \quad (15)$$

Then, we can obtain

$$W = \left[\sum_{n=1}^{5} \alpha_n I_n + (1 - \alpha_1 - \alpha_2 - \alpha_3 - \alpha_4 - \alpha_5) I_6\right]^2. \quad (16)$$

We solve the following equation system $W = $ min can be satisfied

$$\begin{cases} \frac{\partial W}{\partial \alpha_1} = 0 \\ \frac{\partial W}{\partial \alpha_2} = 0 \\ \frac{\partial W}{\partial \alpha_3} = 0. \\ \frac{\partial W}{\partial \alpha_4} = 0 \\ \frac{\partial W}{\partial \alpha_5} = 0 \end{cases} \quad (17)$$

We solve the above equation, and $\alpha_i (i = 1, 2, 3, 4, 5)$ are obtained

$$A' = \left[\sum_{n=1}^{6} \alpha_i A_i\right] \quad B' = \left[\sum_{n=1}^{6} \alpha_i B_i\right]$$

$$C' = \left[\sum_{n=1}^{6} \alpha_i C_i\right] \quad D' = \left[\sum_{n=1}^{6} \alpha_i D_i\right]$$

$$E' = \left[\sum_{n=1}^{6} \alpha_i E_i\right], F' = \left[\sum_{n=1}^{6} \alpha_i F_i\right]. \quad (18)$$

The obtained coefficients A', B', C', D', E', F' form the six coefficients for fitting conic, thereby obtaining the implicit equation. Finally, $\mathbf{Q}'$ is the fitting conic. According to the above process, piecewise fitting is performed on the signal strength at
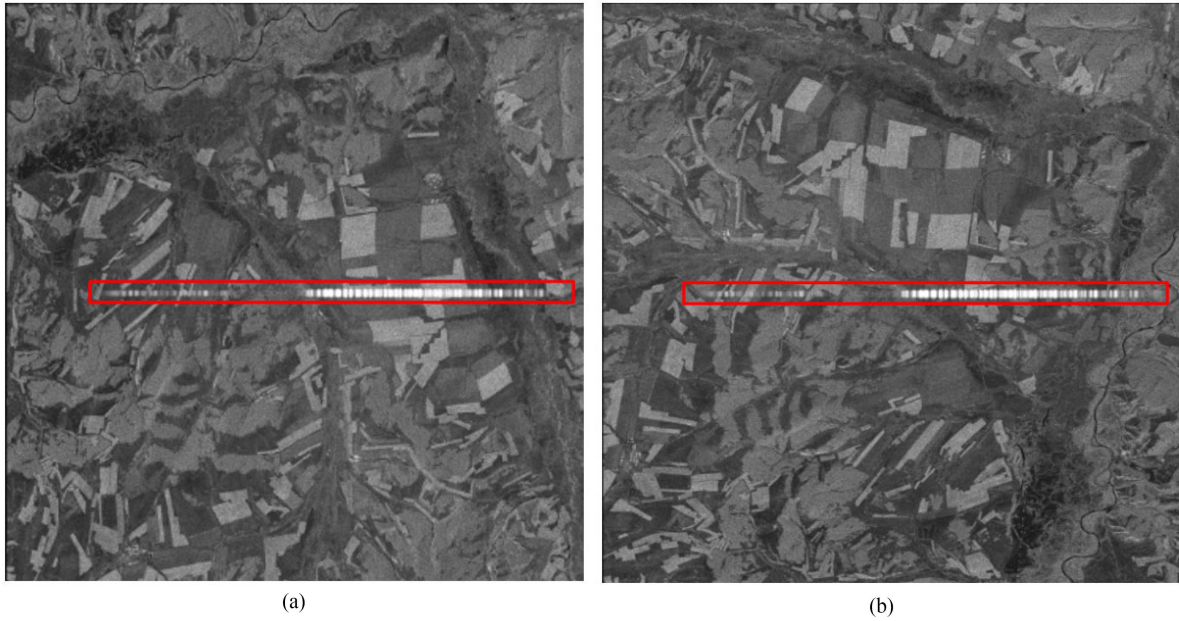
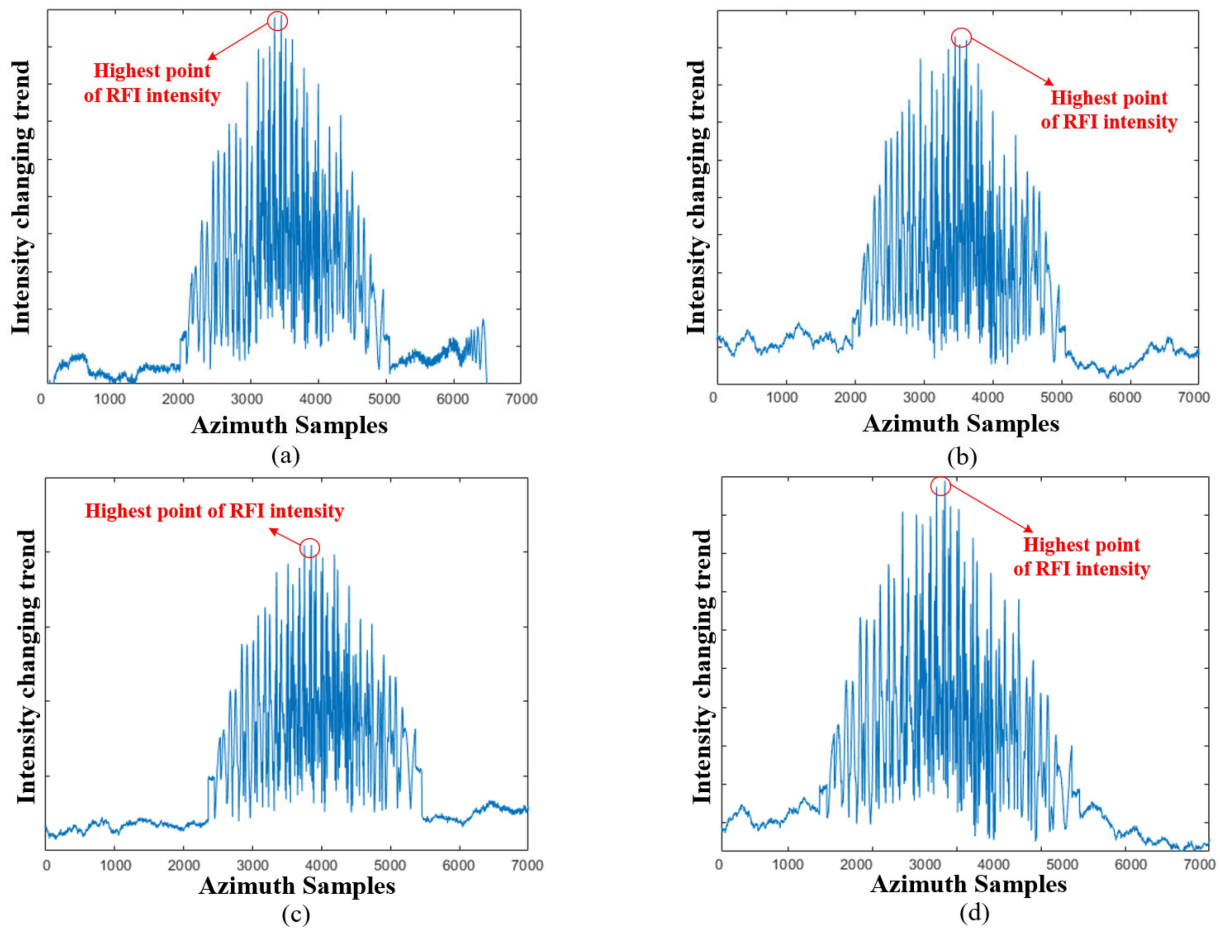Fig. 7.   Image of the target area. (a) Image of the ascending pass. (b) Image of the descending pass.

Fig. 8.   RFI signal change trend images. (a) RFI signal change trend of ascending pass (squint angle: 0°). (b) RFI signal change trend of descending pass (squint angle: 0°). (c) RFI signal change trend of ascending pass (squint angle: 1°). (d) RFI signal change trend of ascending pass (squint angle: 1°).
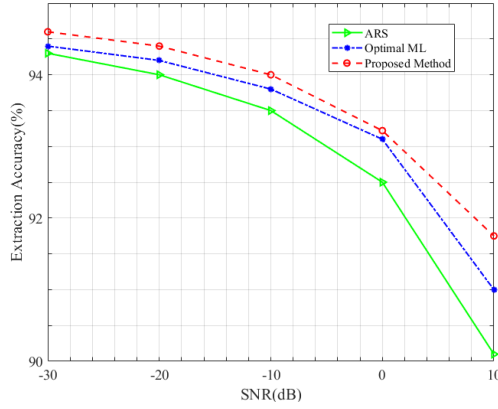
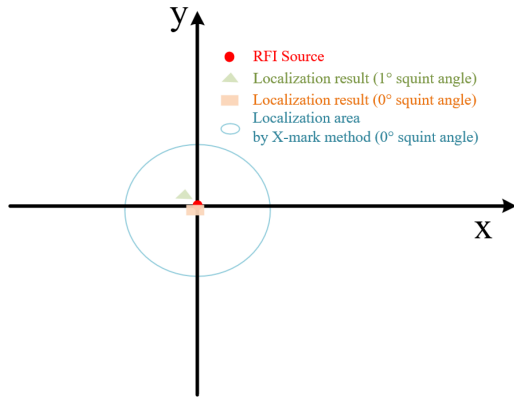Fig. 9. Schematic diagram of RFI extraction accuracy.

Fig. 10. Schematic diagram of localization result.

different azimuth slow time in the data after RFI detection and extraction to obtain the fitting conic.

Then, the LI is first proposed, that is, the location with the highest probability of RFI source. Let the LI be l, then

$$l = N_i / N_a. \qquad (19)$$

When $\mathbf{Q}'$ reaches the maximum value, then $N_i = i$.

$$\max(\mathbf{Q}'), \ N_i = i. \qquad (20)$$

To calculating the LI of the RFI in the raw data of the ascending and descending passes, the RFI detection is performed on the echo signals of the ascending and descending passes in the target area respectively. When there is RFI, subsequent RFI extraction are performed, then the LI of the ascending and descending passes data, l_A and l_D are obtained. At this time, the azimuth location with the highest probability of the RFI source is obtained.

Since SAR imaging is generally in oblique range coordinates, its geometry is corrected into geographic coordinates, so that the image location is consistent with the geographic coordinates. This can transform the vertical or horizontal RFI in images into different directions. Geometric correction processing is the basic operation of SAR image preprocessing, so it will not be repeated here.

Based on the two images of the ascending and descending passes after geometric correction, the two images are intersected

Parameter items	Parameters
Carrier frequency	5.4GHz
Satellite speed	7568m/s
Synthetic aperture length	3.6km
Squint angle	0°/1°
Orbital inclination	112.5°
Slant range	800km

according to the acquisition orbit inclination of the SAR system, so that he partial area of the two images coincide. Then, the following calculation is performed according to the LI l_A and l_D of the RFI in the ascending and descending passes data

$$\mathrm{I}_A = l_A \times \mathrm{X}_A \qquad (21)$$

$$\mathrm{I}_D = l_D \times \mathrm{X}_D. \qquad (22)$$

Among them, X_A and X_D are the number of pixels in azimuth of the two images of the ascending and descending passes, respectively. I_A and I_D are azimuth locations where the RFI source exists in the SAR ascending and descending passes images. The location in azimuth of the two images are intersected, and the intersection point is the precise location of the RFI source.

V. SIMULATION AND EXPERIMENTAL RESULTS

In this article, the effectiveness of the proposed method is verified with experiments based on the raw data of simulation and sentinel-1.

A. Experimental Result Based on Simulation SAR Data

In order to demonstrate the superiority of the proposed algorithm, simulation experiments are conducted in this section. The SAR raw data of ascending and descending passes for the same region are simulated, the RFI source is added to verify the localization accuracy of the proposed algorithm. Fig. 6 shows the geometric model of the simulation experiments. Among them, the parameters of the ascending and descending passes simulation experiments is given in Table I.

The RFI source is added in the center of the scene to simulate the situation. We set the coordinates of the scene center to $O(0,0)$, with the RFI source located in the center of the scene at $(0,0)$. As shown in Fig. 7(a) is the imaging result after simulating the SAR raw data of the ascending pass, and Fig. 7(b) is the imaging result after simulating the SAR raw data of the descending pass. It can be seen that the image are significantly contaminated by RFI.

In SAR systems, there may also be squint angle. This article conducted simulation experiments on the location of RFI source in both side-looking and squint situations. The RFI detection and extraction is performed on simulated raw data.

Then RPW is performed on the signal after RFI detection and extraction in the azimuth slow time, and the LI is calculated. As shown in Fig. 8(a) and (b) represent the strength changes of
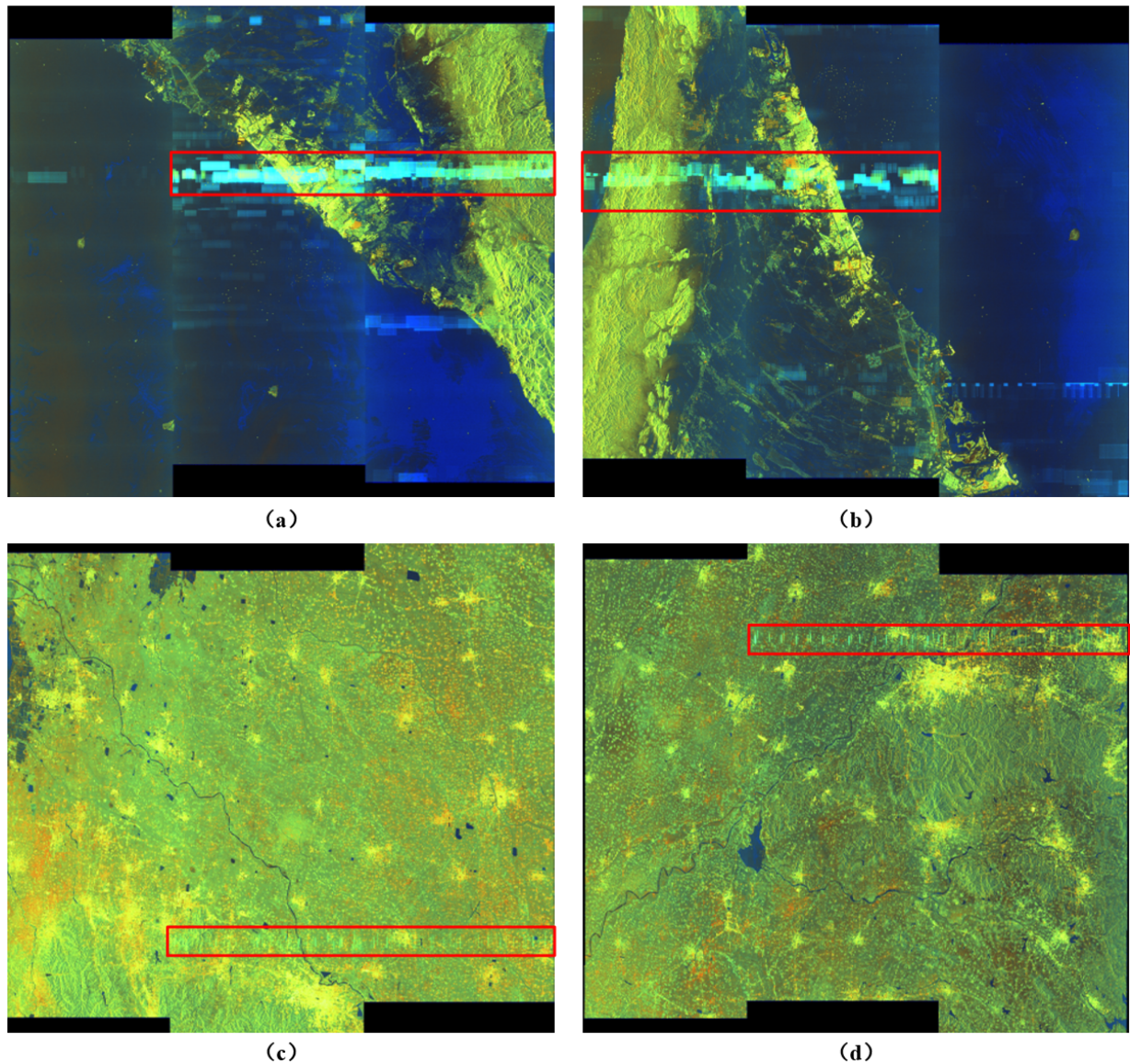
Fig. 11.   Pseudo color image of the target area. (a) Ascending pass pseudo color image in Dubai. (b) Descending pass pseudo color image in Dubai. (c) Descending pass pseudo color image in Jinan. (a) Ascending pass pseudo color image in Jinan.

the ascending and descending passes in the case of side-looking SAR, and Fig. 8(c) and (d) represent the strength changes of the ascending and descending passes in the case of squint SAR, the squint angle is 1°. We analyzed the RFI detection and extraction results, as shown in the Fig. 9. The above detection methods are more suitable for detecting and extracting RFI with higher accuracy, and traditional detection methods are unable to effectively separate RFI and SAR echo. In this case, completing subsequent operations can further improve the accuracy of localization.

Through the algorithm proposed in this article, the final localization result is shown in Fig. 10. It can be seen that the side-looking SAR has good accuracy and coincides with the location of the RFI source. In the case of squint SAR, due to issues such as range migration etc., the results of imaging changes from the actual geographical location, and resulting in a decrease in accuracy. However, there is still a significant improvement compared to traditional algorithms.

As given in Table II, it can be seen that the proposed algorithm has good localization accuracy in both side-looking and squint situations, which is significantly improved compared to traditional algorithms. The traditional X-mark method has limited localization accuracy. When there is a squint angle in the SAR system, the error will increase exponentially, making it almost impossible to locate the target RFI source.

B. Measured Data Description

This article used sentinel-1 raw data. The repeat cycle of sentinel-1 satellite data is 12 days, and its orbital inclination is 98.18 °. Assuming that there is a RFI source on the ground that lasts for a period of time, the geographical location of the RFI source can be determined by using the original data of the ascending and descending passes of sentinel-1 satellite. The two experimental areas used in this article are the raw data of
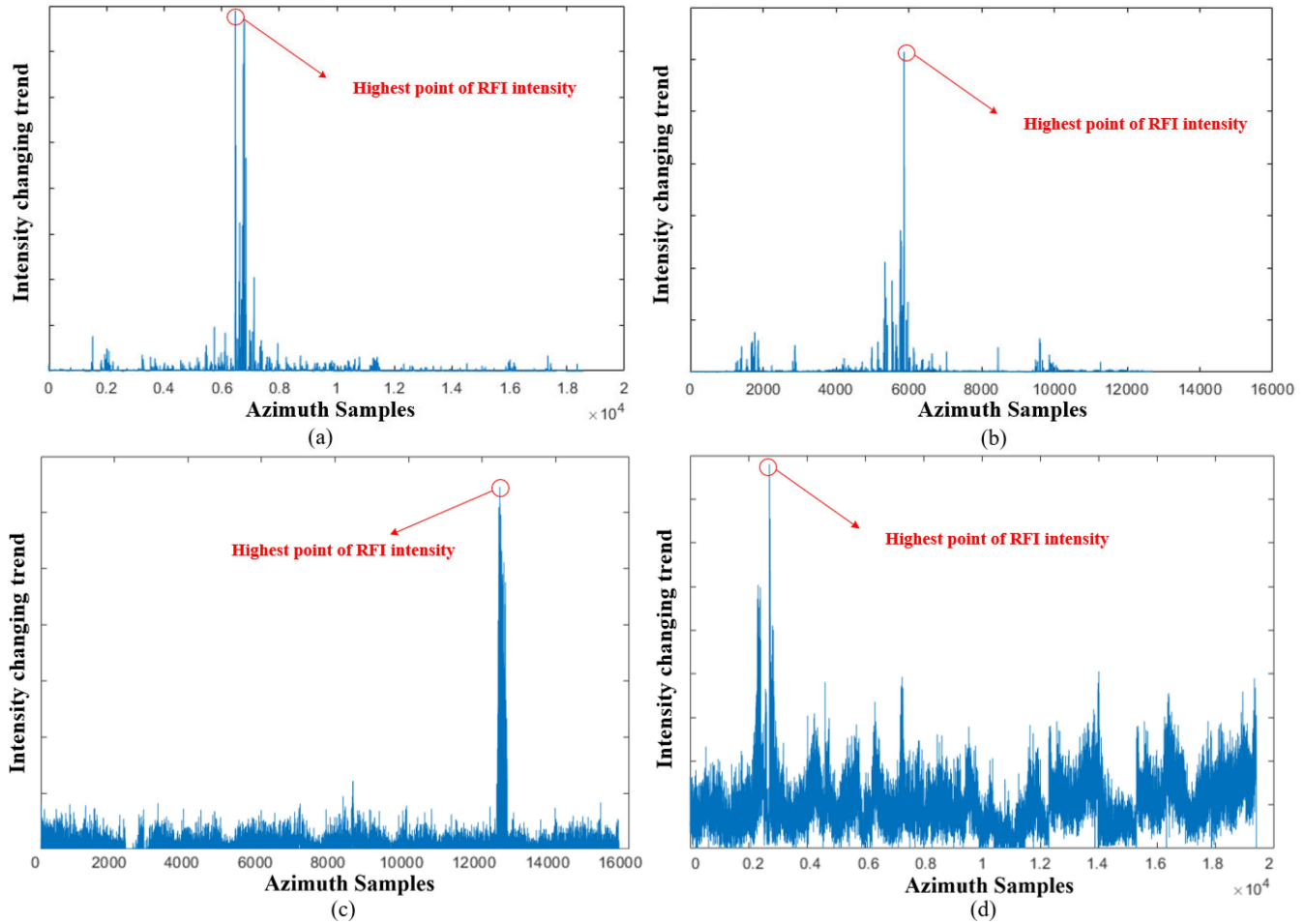
Fig. 12. RFI signal change trend images. (a) RFI signal change trend of ascending pass in Dubai. (b) RFI signal change trend of descending pass in Dubai. (c) RFI signal change trend of descending pass in Jinan. (d) RFI signal change trend of ascending pass in Jinan.

TABLE II
COMPARISON OF LOCALIZATION RESULTS

Squint angle	Method	True RFI location	Estimated RFI location(m)	Localization Accuracy
0°	Proposed method	(0,0)	(0, -0.42)	0.42 m
	Traditional X-mark method	(0,0)	(-1207.7~1207.7, -1207.7~1207.7)	2415.4 m
1°	Proposed method	(0,0)	(-1.6,2.2)	2.7203 m
	Traditional X-mark method	(0,0)	----------	----------

the ascending and descending passes in the Dubai and Jinan regions, respectively. Table III gives detailed information on the data used. Fig. 11 shows the pseudocolor image of the target area, where Fig. 11(a) is the ascending pass image of the Dubai, Fig. 11(b) is the descending pass image of the Dubai, Fig. 11(c) is the descending pass image of the Jinan, and Fig. 11(d) is the ascending pass image of the Jinan In above areas, there is significant RFI in the image of the ascending and descending passes, which persists for a period of time. Therefore, we can conduct research on these data to validate the proposed algorithm in this article. In Fig. 11, it can be clearly seen that there is significant RFI in the red area, and all RFIs are persistent.

C. Experimental Result Based on Measured Data

This article utilizes raw data from the sentinel-1 area to first detect and extract RFI from the raw data, obtaining RFI signals to eliminate the influence of background useful signals on the location of RFI sources. Then, azimuth superposition is performed to fit the changing trend of the RFI signal. As shown in Fig. 12(a)–(d) are the RFI signal changing trend images of the ascending and descending passes data in Dubai and Jinan respectively. It can be seen from the Fig. 12 that the RFI signal strength reaches the highest in a certain sampling time. We believe that the location with the highest RFI signal
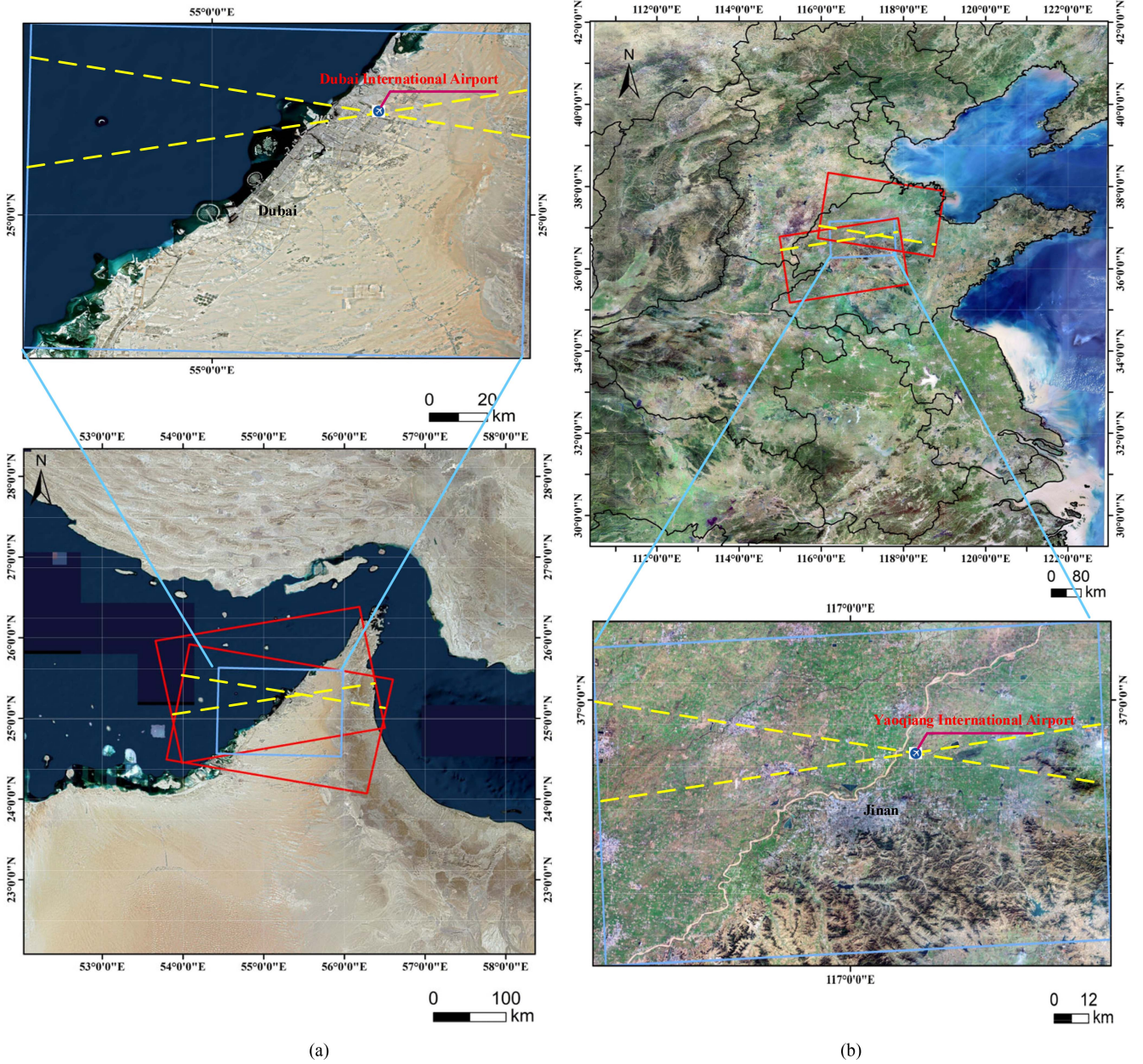
Fig. 13.   Localization results of scene. (a) Localization results of peripheral area in Dubai. (b) Localization results of peripheral area in Jinan.

strength is the closest between the RFI source and the SAR receiver. According to the localization method in Section III of this article, after the raw data imaging, geometric correction is performed, the ascending and descending passes in Dubai and Jinan are intersected according to the geographical location, and the azimuth location of the RFI source is obtained according to the LI. The intersection point is the precise location of the RFI source. As shown in Fig. 13, the localization results of the two regions show that the RFI sources in the Dubai and Jinan regions are located near the airport or city center. The green dashed lines represent the highest probability azimuth location of the RFI source. Generally, we believe that the airport or city center is the area most likely to generate RFI to the SAR system, which is in line with normal cognition. Therefore, the obtained localization results are reliable.

VI. DISCUSSION

In this article, in order to obtain the location of ground RFI source and achieve precise electromagnetic situational aware-ness, an RFI source localization method by integrating SAR raw data both in ascending and descending passes was proposed. Through RFI detection and extraction, RPW and other steps, the LI is obtained to accurately locate the RFI source in SAR data. Through simulation experiments, the localization accuracy has been verified, and the proposed algorithm has better accuracy than the traditional "X-mark" algorithm. The accuracy of this algorithm is closely related to the accuracy of RFI detection and extraction. In an ideal situation, that is, RFI is fully detected and extracted, and without the influence of ground echo data received by SAR receiver, the accuracy can reach the meter-level.

TABLE III
EXPERIMENTAL DATA DESCRIPTION

Image	Image Name	Pass	Sensing time
(a)	S1A_IW_RAW__0SDV_20190708T142445_20190708T142518_028027_032A4E_D49C	Ascending	July 8, 2019
(b)	S1A_IW_RAW__0SDV_20190711T021525_20190711T021551_028063_032B59_1A83	Descending	July 11, 2019
(c)	S1B_IW_RAW__0SDV_20161221T221224_20161221T221256_003500_005FC0_2971	Descending	December 12, 2016
(d)	S1A_IW_RAW__0SDV_20161227T101224_20161227T101256_014564_017A8E_88B2	Ascending	December 27, 2016

Not only that, the proposed algorithm has been applied to sentinel-1 satellite data. In the Dubai and Jinan regions, we analyzed the ascending and descending passes data and found that the RFI source is likely to occur near Dubai International Airport and Jinan Yaoqiang International Airport, the superiority and practical application effects of this algorithm have been demonstrated.

Above all, this article believes that the localization accuracy of the RFI source is related to the resolution of the SAR system. According to the localization method proposed in this article, the RFI source can be located to a certain pixel. In ideal situations (RFI detection and extraction accuracy is close to 100%, without the influence of background signals), the localization accuracy is the azimuth resolution of the SAR system. This article uses sentinel-1 data, which suggests that in ideal situations, the localization accuracy has been a significant improvement. Compared with traditional algorithms, the localization accuracy has been significantly improved.

VII. CONCLUSION

In this article, based on the RFI localization method proposed by Leng et al., we further explore and improve the traditional X-mark method, and an RFI source localization scheme is proposed by integrating ascending and descending passes based on SAR raw data. The LI was first proposed to locate the RFI source after RFI detection and extraction. Subsequently, the location of the RFI source is determined by referring to the LI and the orbit inclination of the satellite-borne SAR based on RPW in azimuth. In an ideal situation, the localization accuracy has been a significant improvement, which greatly improves the localization accuracy compared to the traditional X-mark method.

However, the accuracy of current RFI detection and extraction algorithms is limited, and the proposed algorithm is limited by the influence of useful signals. In the future, further exploration can be made on how to accurately extract and separate RFI signals from useful signals, which can further improve the localization accuracy and universality of the algorithm.

REFERENCES

[1] A. Moreira, P. Prats-Iraola, M. Younis, G. Krieger, I. Hajnsek, and K. P. Papathanassiou, "A tutorial on synthetic aperture radar," *IEEE Geosci. Remote Sens. Mag.*, vol. 1, no. 1, pp. 6–43, Apr. 2013.

[2] Y. Deng, W. Yu, H. Zhang, W. Wang, D. Liu, and R. Wang, "Forthcoming spaceborne SAR development," *J. Radars*, vol. 9, no. 1, pp. 1–33, Feb. 2020.

[3] M. Datcu, Z. Huang, A. Anghel, J. Zhao, and R. Cacoveanu, "Explainable, physics-aware, trustworthy artificial intelligence: A paradigm shift for synthetic aperture radar," *IEEE Geosci. Remote Sens. Mag.*, vol. 11, no. 1, pp. 8–25, Mar. 2023.

[4] X. Zhu et al., "Deep Learning meets SAR: Concepts, models, pitfalls, and perspectives," *IEEE Geosci. Remote Sens. Mag.*, vol. 9, no. 4, pp. 143–172, Dec. 2021.

[5] X. Leng, K. Ji, S. Zhou, X. Xing, and H. Zou, "Discriminating ship from radio frequency interference based on noncircularity and non-Gaussianity in Sentinel-1 SAR imagery," *IEEE Trans. Geosci. Remote Sens.*, vol. 57, no. 1, pp. 352–363, Jan. 2019.

[6] X. Leng, K. Ji, B. Xiong, and G. Kuang, "Complex signal kurtosis—Indicator of ship target signature in SAR images," *IEEE Trans. Geosci. Remote Sens.*, vol. 60, May 2021, Art. no. 5208312.

[7] H. Yang et al., "Robust block subspace filtering for efficient removal of radio interference in synthetic aperture radar images," *IEEE Trans. Geosci. Remote Sens.*, vol. 62, Feb. 2024, Art. no. 5206812.

[8] M. Tao, J. Su, Y. Huang, and L. Wang, "Mitigation of radio frequency interference in synthetic aperture radar data: Current status and future trends," *Remote Sens.*, vol. 11, no. 20, Oct. 2019, Art. no. 2438.

[9] B. Zhang, G. Xu, R. Zhou, H. Zhang, and W. Hong, "Multi-channel back-projection algorithm for mmWave automotive MIMO SAR imaging with Doppler-division multiplexing," *IEEE J. Sel. Topics Signal Process.*, vol. 17, no. 2, pp. 445–457, Mar. 2023.

[10] B. Peng, B. Peng, J. Zhou, J. Xie, and L. Liu, "Scattering model guided adversarial examples for SAR target recognition: Attack and defense," *IEEE Trans. Geosci. Remote Sens.*, vol. 60, Oct. 2022, Art. no. 5236217.

[11] Y. Tan et al., "Joint communication and SAR waveform design method via time-frequency spectrum shaping," *IEEE Trans. Geosci. Remote Sens.*, vol. 60, Dec. 2022, Art. no. 5241313.

[12] ARESYS, "2021 S-1 RFI maps," *Aresys Earth Observation*, Jun. 2021. [Online]. Available: https://s1rfimap.aresys.it

[13] J. R. Yang, "Measurement of amplitude and phase differences between two RF signals by using signal power detection," *IEEE Microw. Wireless Compon. Lett.*, vol. 24, no. 3, pp. 206–208, Jan. 2014.

[14] K. C. HO, "Bias reduction for an explicit solution of source localization using TDOA," *IEEE Trans. Signal Process.*, vol. 60, no. 5, pp. 2101–2114, May 2012.

[15] K. C. Ho, X. Lu, and L. Kovavisaruch, "Source localization using TDOA and FDOA measurements in the presence of receiver location errors: Analysis and solution," *IEEE Trans. Signal Process.*, vol. 55, no. 2, pp. 684–696, Feb. 2007.

[16] S. Zhang and M. Xing, "A novel doppler chirp rate and baseline estimation approach in the time domain based on weighted local maximum-likelihood for an MC-HRWS SAR system," *IEEE Geosci. Remote Sens. Lett.*, vol. 14, no. 3, pp. 299–303, Mar. 2017.

[17] M. Trinh-Hoang, M. Viberg, and M. Pesavento, "Partial relaxation approach: An eigenvalue-based DOA estimator framework," *IEEE Trans. Signal Process.*, vol. 66, no. 23, pp. 6190–6203, Dec. 2018.

[18] H. Park, V. González-Gambau, and A. Camps, "High angular resolution RFI localization in synthetic aperture interferometric radiometers using direction-of-arrival estimation," *IEEE Geosci. Remote Sens. Lett.*, vol. 12, no. 1, pp. 102–106, Jun. 2014.

[19] A. G. Dempster and E. Cetin, "Interference localization for satellite navigation systems," *Proc. IEEE*, vol. 104, no. 6, pp. 1318–1326, Mar. 2016.

[20] J. Li, F. Hu, F. He, and L. Wu, "High-resolution RFI localization using covariance matrix augmentation in synthetic aperture interferometric radiometry," *IEEE Trans. Geosci. Remote Sens.*, vol. 56, no. 2, pp. 1186–1198, Oct. 2017.

[21] J. W. Steeb, D. B. Davidson, and S. J. Wijnholds, "Computationally efficient radio frequency source localization for radio interferometric arrays," *Radio Sci.*, vol. 53, no. 3, pp. 242–256, Mar. 2018.

[22] R. Jin, L. Wu, Q. Li, H. Lu, and L. Feng, "Geolocation of RFIs by multiple snapshot difference method for synthetic aperture interferometric radiometer," *IEEE Trans. Geosci. Remote Sens.*, vol. 60, Jan. 2022, Art. no. 4700112.

[23] D. Zhu, J. Li, and G. Li, "RFI source localization in microwave interferometric radiometry: A sparse signal reconstruction perspective," *IEEE Trans. Geosci. Remote Sens.*, vol. 58, no. 6, pp. 4006–4017, Jun. 2020.

[24] D. Zhu, X. Peng, and G. Li, "A matrix completion based method for RFI source localization in microwave interferometric radiometry," *IEEE Trans. Geosci. Remote Sens.*, vol. 59, no. 9, pp. 7588–7602, Sep. 2021.

[25] L. Zhang, H. Huan, R. Tao, and Y. Wang, "Emitter localization algorithm based on passive synthetic aperture," *IEEE Trans. Aerosp. Electron. Syst.*, vol. 58, no. 4, pp. 2687–2701, Aug. 2022.

[26] A. Li, H. Huan, R. Tao, and L. Zhang, "Passive synthetic aperture high-precision radiation source location by single satellite," *IEEE Geosci. Remote Sens. Lett.*, vol. 19, Feb. 2021, Art. no. 4010105.

[27] Y. Wang, G. Sun, J. Yang, M. Xing, X. Yang, and Z. Bao, "Passive localization algorithm for radiation source based on long synthetic aperture," *J. Radars*, vol. 9, no. 1, pp. 185–194, 2020.

[28] K. A. Sørensen, A. Kusk, P. Heiselberg, and H. Heiselberg, "Finding ground-based radars in SAR images: Localizing radio frequency interference using unsupervised deep learning," *IEEE Trans. Geosci. Remote Sens.*, vol. 61, Jul. 2023, Art. no. 4704215.

[29] H. Yang, J. Yang, and Z. Liu, "Localizing ground-based pulse emitters via synthetic aperture radar: Model and method," *IEEE Trans. Geosci. Remote Sens.*, vol. 61, Sep. 2023, Art. no. 5216714.

[30] ARESYS, "Sentinel-1 RFI maps," Jun. 2019. [Online]. Available: https://s1rfimap.aresys.it

[31] C. J. Banks et al., "Reduced ascending/descending pass bias in SMOS salinity data demonstrated by observing westward-propagating features in the South Indian Ocean," *Remote Sens. Environ.*, vol. 180, pp. 154–163, 2016.

[32] V. Kumar, G. Venkataramana, and K. A. Høgda, "Glacier surface velocity estimation using SAR interferometry technique applying ascending and descending passes in Himalayas," *Int. J. Appl. Earth Obs. Geoinf.*, vol. 13, no. 4, pp. 545–551, 2011.

[33] D. Harel, "X marks the spot: Identifying MIM-104 Patriot batteries from Sentinel-1 SAR multi temporal imagery," *Medium*, Oct. 2018. [Online]. Available: https://medium.com/@HarelDan/x-marks-the-spot-579cdb1f534b

[34] X. Leng, K. Ji, and G. Kuang, "Radio frequency interference detection and localization in sentinel-1 images," *IEEE Trans. Geosci. Remote Sens.*, vol. 59, no. 11, pp. 9270–9281, Nov. 2021.

Ning Li (Member, IEEE) received the B.S. degree in electronics information engineering from Northeast Forestry University, Harbin, China, in 2009, the M.S. degree in communication and information system from the Nanjing University of Aeronautics and Astronautics, Nanjing, China, in 2012, and the Ph.D. degree in communication and information systems from the Institute of Electronics, Chinese Academy of Sciences (IECAS), Beijing, China, in 2015.

In 2015, he was with the Department of Space Microwave Remote Sensing System, IECAS, Beijing, China, where he was an Assistant Professor. Since 2017, he has been a Full Professor with the School of Computer and Information Engineering, Henan University, Kaifeng, China. His research interests include synthetic aperture radar (SAR) and inverse SAR imaging algorithms and autofocusing techniques, SAR polarimetric theory, and SAR image processing.

Dr. Li was a recipient of the Special Prize of President Scholarship for Postgraduate Students from the University of Chinese Academy of Sciences in 2015.

Zhengwei Guo received the B.S. degree in radio technology engineering from the Huazhong University of Science and Technology, Wuhan, China, in 1984.

She was an Assistant Professor Henan University, Kaifeng, China, where she has been a Professor with the School of Computer and Information Engineering since 2008. Her projects on synthetic aperture radar (SAR) image applications and information processing system have been supported by the National Natural Science Foundation of China and the Department of Science and Technology of Henan Province. She has authored or coauthored several papers, including peer-reviewed journals, conference proceedings, patents, and software copyrights. Her research focus on management system software, data process systems, and information security technology.

Ms. Guo was the recipient of the First-Prize Scientific and Technological Progress Award of Henan Province.

Zewen Fu was born in Henan, China, in 1996. He received the M.S. degree in software engineering in 2022 from Henan University, Kaifeng, China, where he is currently working toward the Ph.D. degree in software engineering with the School of Computer and Information Engineering.

His research interests include synthetic aperture radar (SAR) signal processing and SAR electronic countermeasure.